Chapter 7: TRIBOLOGICAL PERFORMANCE OF Ni ALLOY-BASED COMPOSITES CONTAINING FIXED AMOUNTS OF Ag, rGO-Ni, AND DIFFERENT AMOUNTS OF *h*-BN-Ni

This chapter presents with the results on the characterization of ball-milled powders and composites, followed by the microstructural and properties evaluation of Ni-alloy based composites containing a combination of fixed amount of Ag (10 wt.%), rGO-Ni (1.0 wt.%) and different amounts of Ni doped *h*-BN (2, 4, 6, and 8 wt.%), namely, NANGh2, NANGh4, NANGh6, and NANGh8. This is followed by the results on the friction and wear behaviour tribo-performance and examination of worn surfaces of above-mentioned composites. The observed friction and wear behaviour has been discussed in the light of worn surface morphology and the probable mechanisms of wear have been highlighted.

7.1 RESULTS

7.1.1 Characterization of Composites

7.1.1.1 Morphology of ball-milled powders and composites

A significant change in the morphology of the mixed powders could be seen as compared to elemental powders (Fig. 4.6) after the ball milling of as judged from Fig. 7.1. The average size of flattened particles has been found to decrease from 47 to 33 μm with an increase in the amount of *h*-BN-Ni from 2 to 8 wt.% as seen from Figs. 7.1 (a-d).

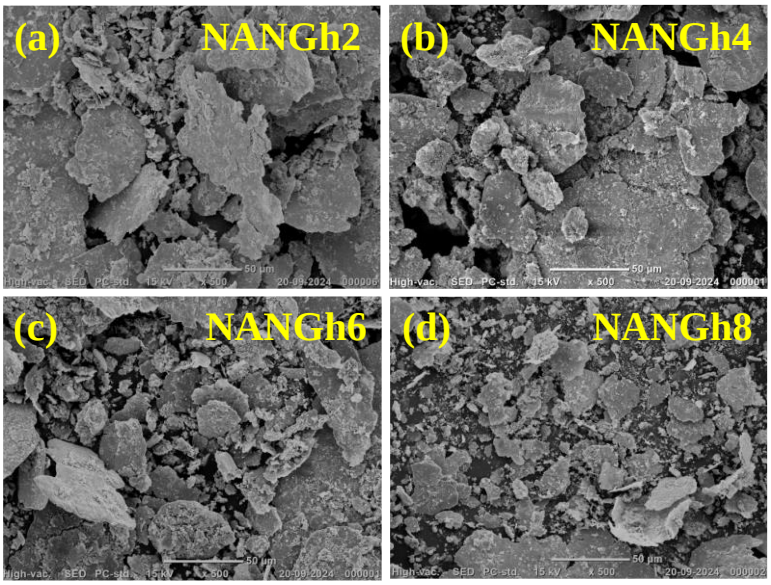

Fig. 7. 1 FESEM micrographs of milled powders (a) NANGh2, (b) NANGh4, (c) NANGh6, and (d) NANGh8

The XRD patterns for milled powders and sintered nanocomposites are depicted in Figs. 7.2 (a and b). XRD patterns of NANGh2, NANGh4, NANGh6, and NANGh8 have revealed the peaks corresponding to Ni (ICSD 98-026-0169), Cr (ICSD 00-006-0694), Mo (ICSD 98-017-3127), Ag (ICSD 01-087-0597), *h*-BN (ICSD 01-085-12068) as shown in Fig. 7.2 (a). One may also observe a peak pertaining to (111) plane of MoC (ICSD 98-007-7157), which may have formed due to a reaction between Mo and rGO. However, no peak corresponding to rGO could be seen, probably due to the very small amount of rGO. The peaks corresponding to constituents of the nanocomposites only i.e., Ni, Cr, Mo, Ag, MoC, and *h*-BN could also be observed in the XRD patterns of the sintered composites with a slight shift of angles as illustrated in Fig. 7.2 (b) which reflects the non-occurrence of any kind of oxidation during the sintering.

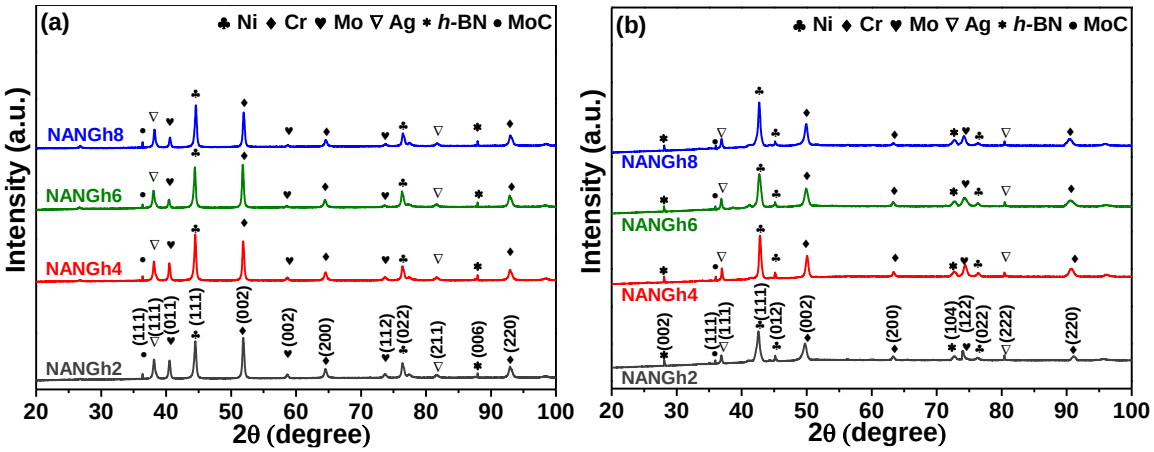

Fig. 7. 2 X-ray diffraction patterns of (a) ball milled powder and (b) spark plasma sintered composite for NANGh2, NANGh4, NANGh6, and NANGh8

7.1.1.2 Microstructure of composites

The microstructure and elemental distribution of the nanocomposites containing Ag, rGO, and *h*-BN are shown in Fig. 7.3. It can be seen clearly that the white areas are Ag and Mo-rich phase, whereas the dark grey areas are Ni alloy matrix phase. The distribution of the elements in the composites such as NANGh2, NANGh4, NANGh6, and NANGh8 is almost similar as seen from their elemental mapping. However, NANGh8 exhibits a nonhomogeneous distribution of Ag and Mo in the microstructure compared to others as shown in Fig. 7.3 (a-d).

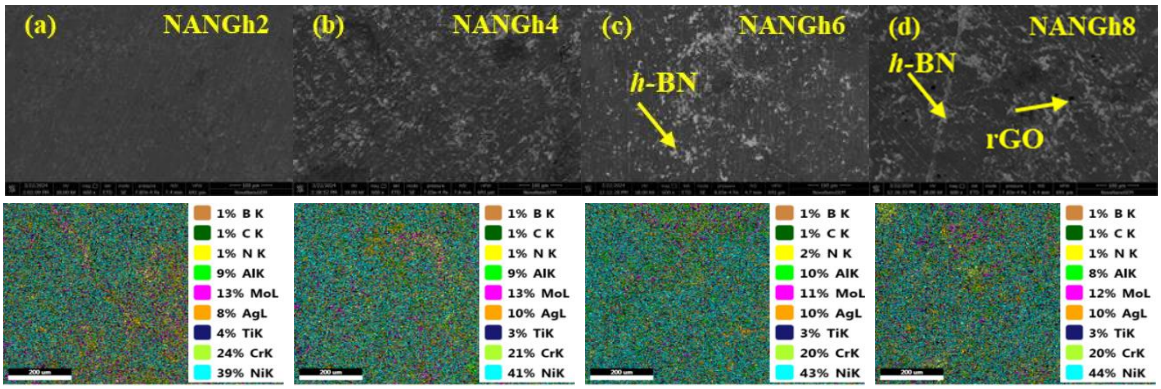

Fig. 7. 3 Scanning Electron micrographs of (a) NANGh2, (b) NANGh4, (c) NANGh6, and (d) NANGh8 along with their corresponding area elemental distribution (Ni, Cr, Mo, Ti, Al, Ag, B, N, C) and wt.% of each element

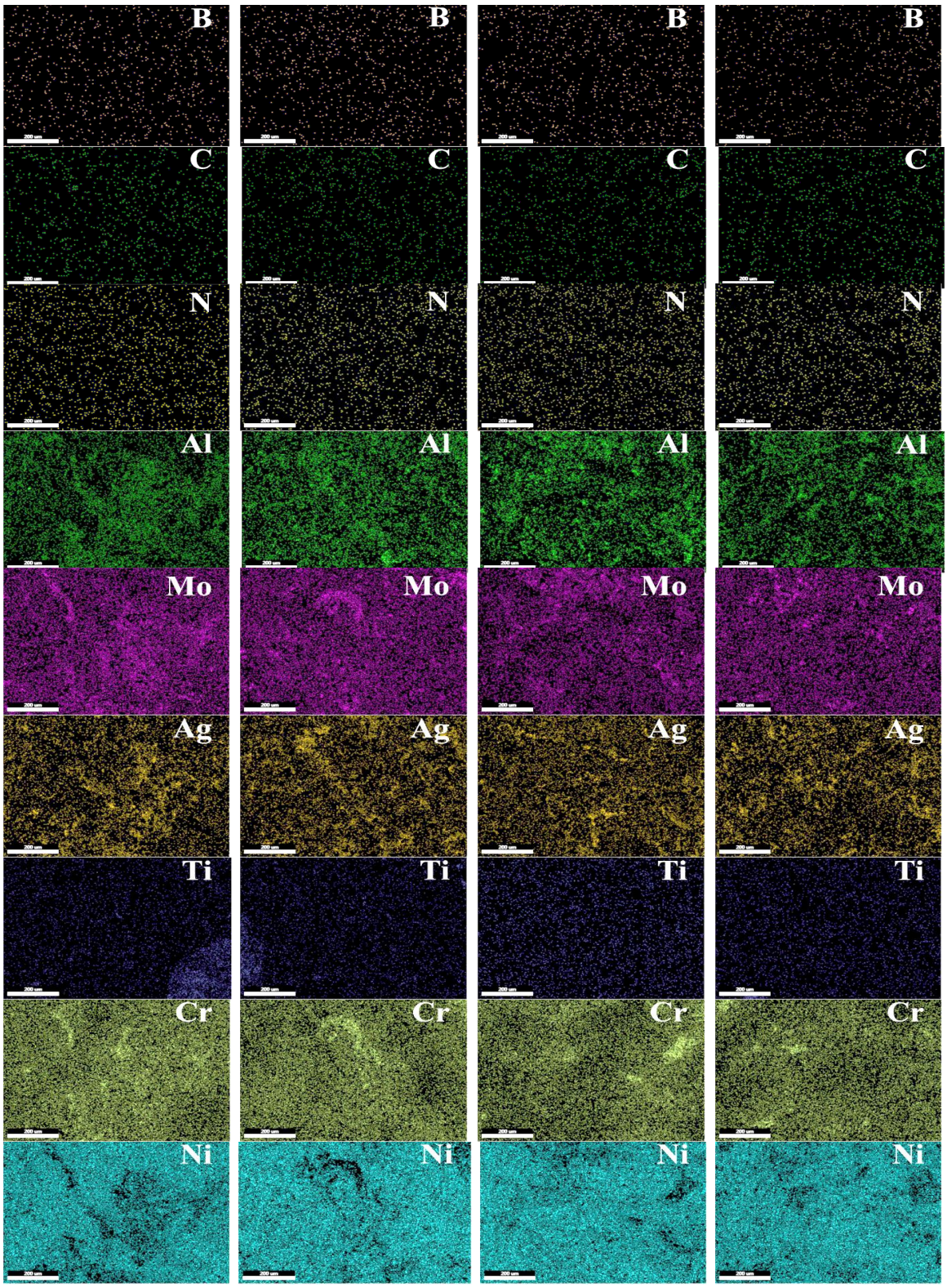
B
B
B
B
C
C
C
C
N
N
N
N
Al
Al
Al
Al
Mo
Mo
Mo
Mo
Ag
Ag
Ag
Ag
Ti
Ti
Ti
Ti
Cr
Cr
Cr
Cr
Ni
Ni
Ni
Ni

Fig. 7.3 Contd.

7.1.1.3 Hardness and density measurement of composites

The microhardness of the sintered composites, namely, NANGh2, NANGh4, NANGh6, and NANGh8 has been measured as 458 ± 3, 433 ± 2, 420 ± 1, and 412 ± 2 $HV_{0.3}$. One may observe the reduction in the hardness of the composites by increasing the amount of *h*-BN.

Table 7. 1 Specimen designation, composition, density, and microhardness

Designation	Composition	Real density (g/cm^3)	Microhardness $HV_{0.3}$ (GPa)
NANGh2	Ni alloy-10 wt.% Ag-1 wt.% rGO-2 wt.% *h*-BN	8.46	458 ± 3
NANGh4	Ni alloy-10 wt.% Ag-1 wt.% rGO-4 wt.% *h*-BN	7.13	433 ± 2
NANGh6	Ni alloy-10 wt.% Ag-1 wt.% rGO-6 wt.% *h*-BN	7.68	420 ± 1
NANGh8	Ni alloy-10 wt.% Ag-1 wt.% rGO-8 wt.% *h*-BN	7.40	412 ± 2

7.1.2 Dry Sliding Friction and Wear Behaviour

7.1.2.1 Variation of coefficient of friction with time

The variation of coefficient of friction (CoF) with time for all the composites at RT, 200, 400, 600, and 800 ºC is shown in Fig. 7.4. The relatively higher CoF with large fluctuations in amplitude with time for N0, NA, and NANG at all the temperatures can be observed compared to the composites containing Ag alone and a combination of fixed amounts of Ag and rGO, which has already been explained in Chapter 4. At RT, the CoF for NANGh2, NANGh4, NANGh6, and NANGh8 is found to stabilize after 215, 223, 304, and 109 seconds, respectively, with relatively large fluctuations in amplitude for NANGh6 as shown in Fig. 7.4 (a). At 200 ºC, the CoF is found to stabilize after 251, 150, 114, and 152 seconds for NANGh2, NANGh4, NANGh6, and NANGh8, respectively, with

comparatively larger fluctuations for NANGh6 and NANGh8 compared to others as depicted in Fig. 7.4 (b). Likewise, at 400 ºC, the CoF is observed to stabilize after 221, 22, 224, and 111 seconds for NANGh2, NANGh4, NANGh6, and NANGh8, respectively, with comparatively larger fluctuations for NANGh6 and NANGh8 as depicted in Fig. 7.4 (c). At 600 ºC, the CoF is found to stabilize after 198, 202, 250, and 80 seconds for NANGh2, NANGh4, NANGh6, and NANGh8, respectively, with comparatively larger fluctuations for NANGh6 and NANGh8 as depicted in Fig. 7.4 (d). However, the relatively short run-in-periods of 100, 120, 52, and 62 seconds are observed for NANGh2, NANGh4, NANGh6, and NANGh8, respectively, at 800 ºC, with relatively larger fluctuations for NANGh4 compared to others as seen from Fig. 7.4 (e). The NANGh8 having 8 wt.% of *h*-BN has shown the lowest CoF with negligible running-in duration in comparison to others at all the temperatures.

7.1.2.2 Variation of average coefficient of friction with temperature

The variation of average CoF with temperature for base alloy (N0) and composites, NA, NANG, NANGh2, NANGh4, NANGh6, and NANGh8 is shown in Fig. 7.5. The average CoF for the specimens has been assessed by discarding the running-in-period. The CoF for N0 and NA has been found to decrease consistently from RT to 800 ºC, whereas CoF for NANG is observed to decrease from RT to 200 ºC and increase from 600 to 800 ºC while remaining almost same in-between 200 to 600 ºC. The CoF for NANGh2 decreases from RT to 800 ºC with a relatively sharp decrease from RT to 200 ºC. A similar trend of variation has been observed for NANGh4. However, the CoF for NANGh6 and NANGh8 has been found to decrease consistently from RT to 800 ºC and NANGh8 has shown the lowest CoF (~ 0.27- 0.17) at all the temperatures.

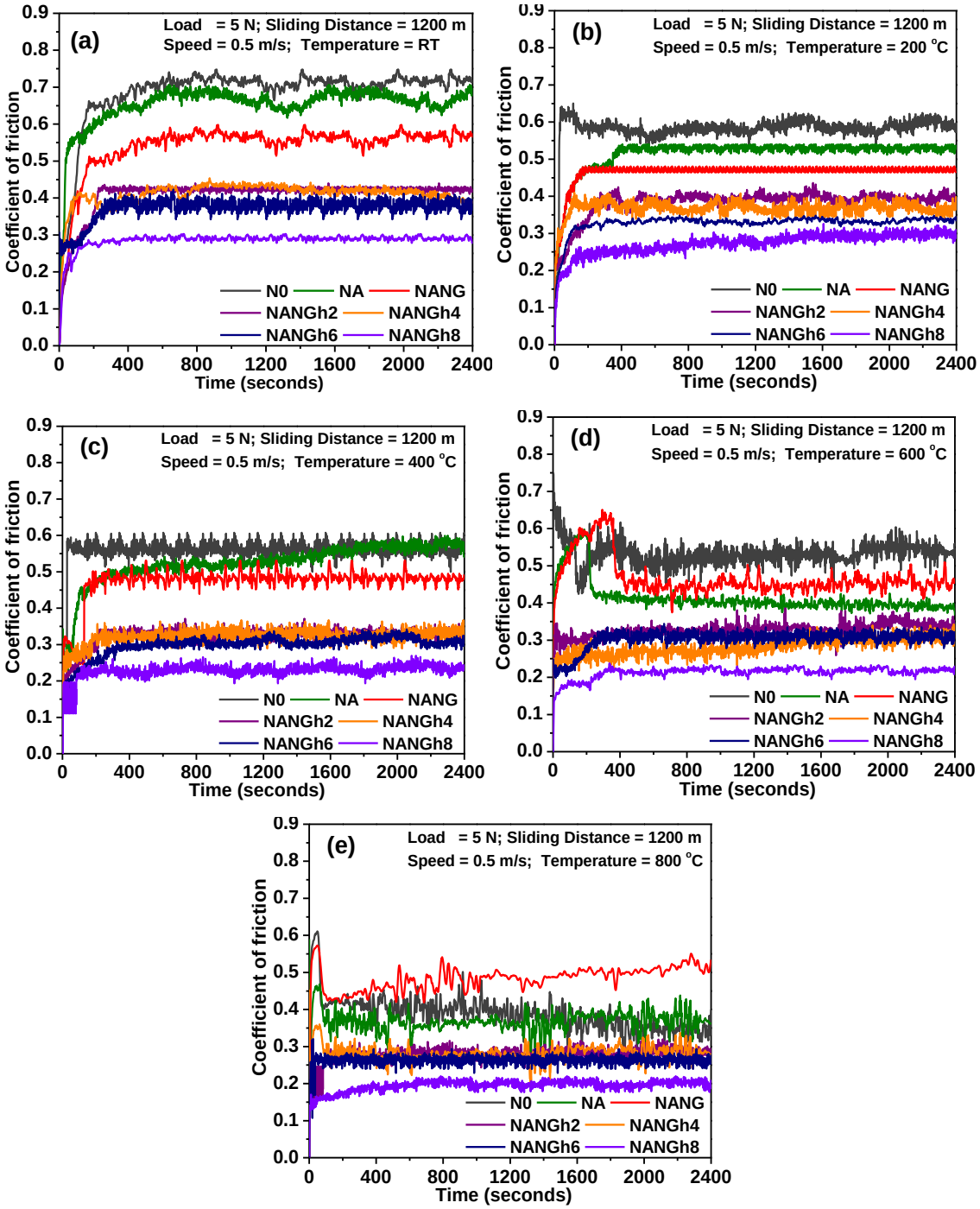

Fig. 7. 4 Variation of coefficient of friction with time at (a) RT, (b) 200, (c) 400, (d) 600, and (e) 800 °C for base alloy and composites

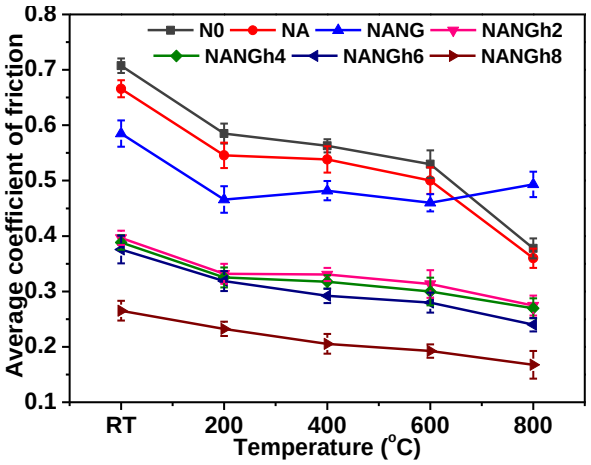

Fig. 7. 5 Variation of average coefficient of friction with temperature for the base alloy and composites

7.1.2.3 Variation of wear rate with temperature

Figure 7.6 depicts the variation of wear rate with temperature for base alloy (N0) and composites such as NA, NANG, NANGh2, NANGh4, NANGh6, and NANGh8. A relatively higher wear rate can be observed for N0, NA, and NANG compared to composites containing Ag, rGO, and *h*-BN at all the temperatures except 400 and 600 ºC, where NANG has been found to exhibit the lowest wear rate. The wear rate for NANGh2 has been observed to increase from RT to 400 ºC and decrease afterwards with a sharp reduction from 600 to 800 ºC. A similar trend of variation in wear rate could also be seen for NANGh4, NANGh6, and NANGh8. The wear rate of the composites is observed to decrease till the addition of *h*-BN from 2 to 6 wt.% and increase at the 8 wt.% addition of *h*-BN. However, NANGh6 shows the lowest wear rate at all the temperatures except at 400 and 600 ºC, where NANG has the lowest wear rate. As part of the tribological system, mass loss of the counterface ball slid against composites at all the temperature was measured using a microbalance. However, due to negligible mass loss, the wear rate of the counterface balls has not been reported here.

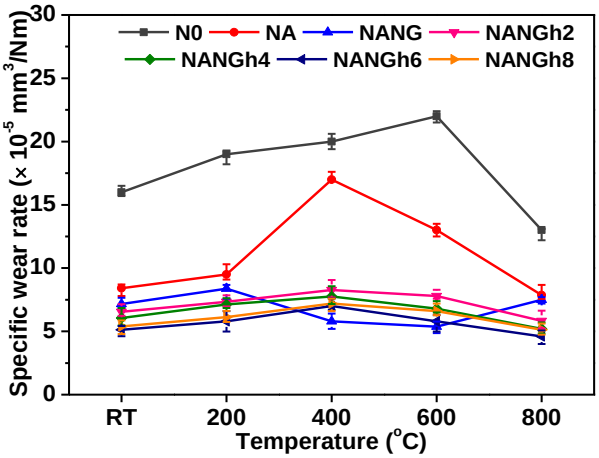

Fig. 7. 6 Variation of specific wear rate with temperature for the base alloy and composites

7.1.3 Morphology of Worn Surfaces

7.1.3.1 Electron microscopy of worn surfaces of tribo-pairs

The FESEM micrographs of the worn surface for NANGh2 at RT, 200, 400, 600, and 800 ºC, along with their EDS have been presented in Figs. 7.7 (a-j). At RT, the worn surface of NANGh2 reveals the presence of a loosely bound tribo-layer covering almost the entire surface, whereas few loose wear particles along with a relatively compact tribo-layer can be observed on the worn surface at 200 ºC as shown in Figs. 7.7 (a and c). A well-compacted and scattered tribo-layer with a few locations of delamination can be seen on the worn surface at 400 ºC as depicted in Fig. 7.7 (e). The delamination allows the direct contact between mating pairs, which may lead to an increase in material loss. However, the presence of a glaze layer which might have formed due to tribo-chemical reactions at 600 and 800 ºC could be observed on the worn surfaces as seen in Figs. 7.7 (g and i). EDS analyses of the square regions marked in Figs. 7.7 (a, c, e, g, and i) reveal the presence of constituent elements of the base alloy and oxygen along with their respective amounts depending on the temperature, indicating the possibility of oxidation as evident from EDS shown in Figs. 7.7 (b, d, f, h, and j)

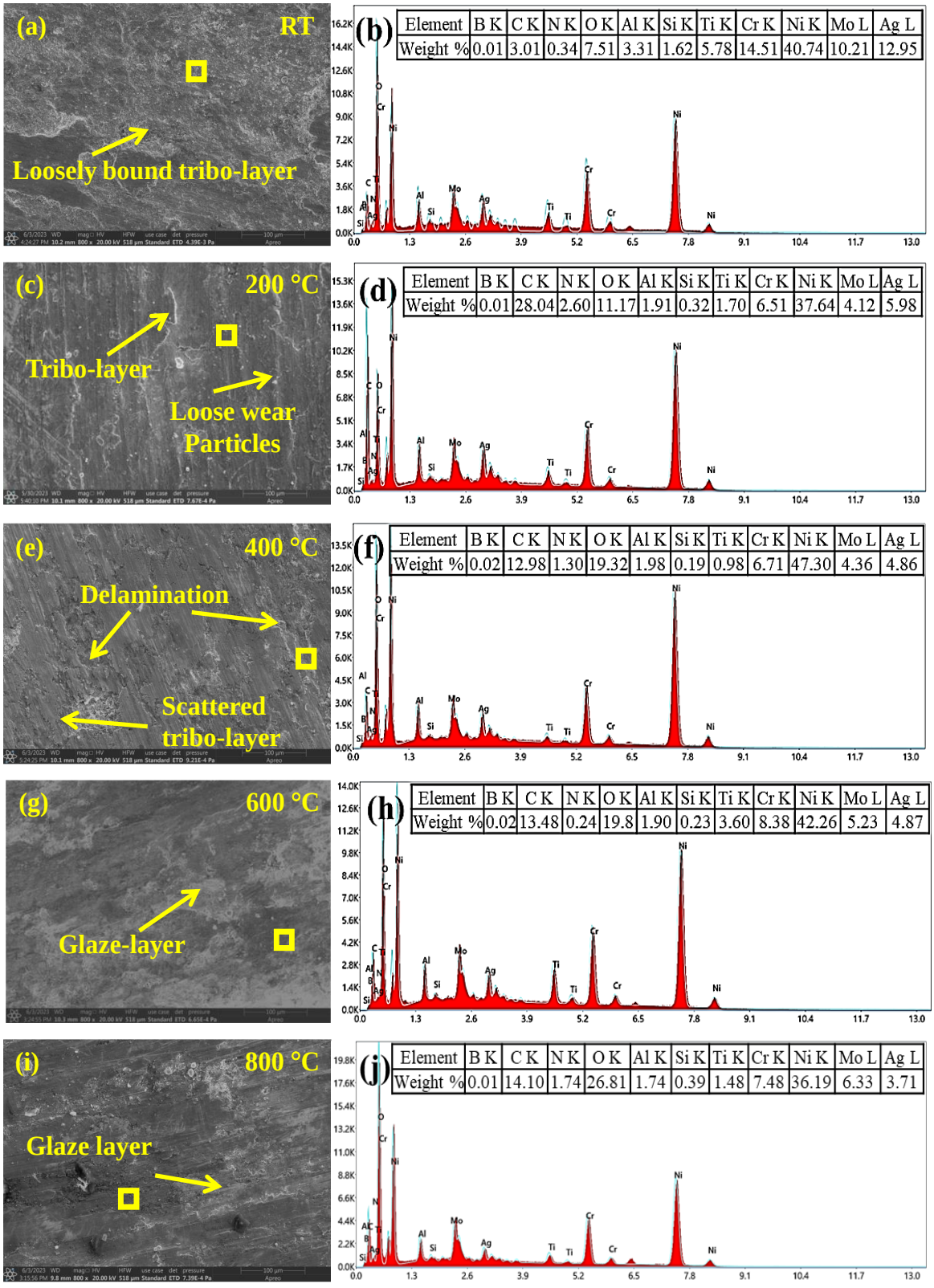

Fig. 7. 7 FESEM micrographs of the worn-out NANGh2 and EDS of the marked region at (a and b) RT, (c and d) 200, (e and f) 400, (g and h) 600, and (i and j) 800 °C

The morphology of the worn surfaces of the ball slid against NANGh2 at RT, 400, and 800 ºC is shown in Figs. 7.8 (a-c). A few wear particles appear to have accumulated at the leading edge of the ball at RT as seen in Fig. 7.8 (a). The presence of a relatively compact and smooth transfer layer can be observed at leading edge of the ball at 400 and 800 ºC as compared to that seen at RT.

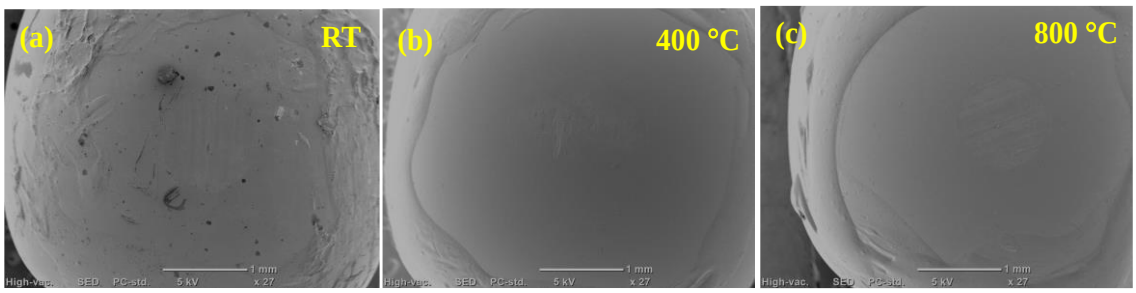

Fig. 7. 8 FESEM micrographs of the worn-out silicon nitride ball (counterface) slid against NANGh2 at (a) RT, (b) 400, and (c) 800 °C

The FESEM micrographs of the worn surface for NANGh4 at RT, 200, 400, 600, and 800 ºC have been shown in Figs. 7.9 (a-j). The surface worn at RT reveals the presence of a compacted tribo-layer covering the sliding marks along with some loose wear particles, whereas a relatively shallow ploughing marks, loose wear particle, and the tribo-layer could be seen on surface worn at 200 ºC as given in Figs. 7.9 (a and c). A relatively more compact and scattered tribo-layer with patches of delamination can be observed on the worn surface at 400 ºC compared to that seen at 200 ºC as illustrated in Figs. 7.9 (c and e). However, the presence of a protective glaze layer of varying degrees of compaction can be observed on the surfaces worn at 600 and 800 ºC as seen in Figs. 7.9 (g and i). The EDS analyses of the square regions marked in Figs. 7.9 (a, c, e, g, and i) reveal the presence of constituent elements of the composite and oxygen along with their respective amounts depending on the temperature indicating towards the possibility of oxidation as seen from Figs. 7.9 (b, d, f, h, and j).

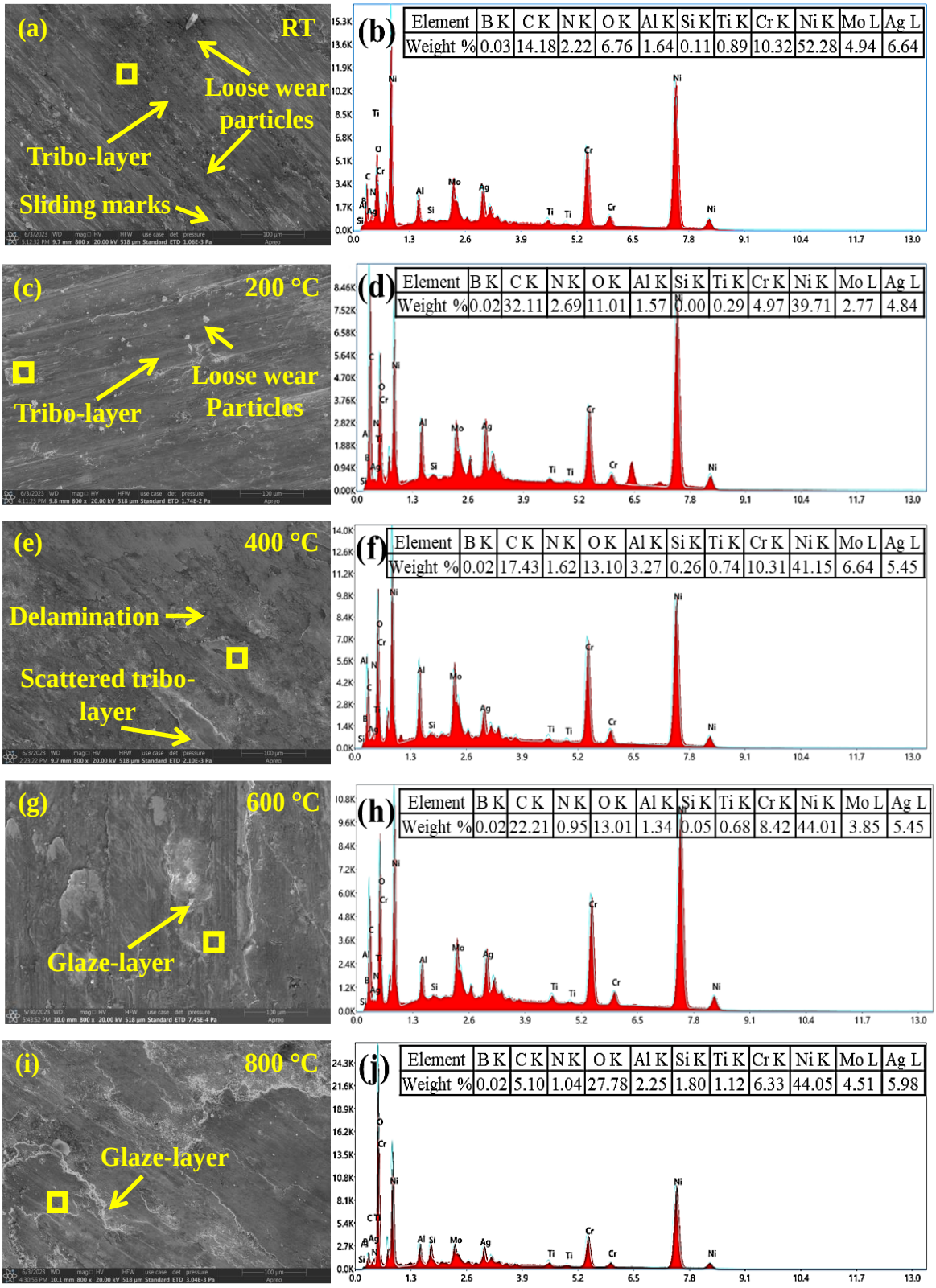

Fig. 7. 9 FESEM micrographs of the worn-out NANGh4 and EDS of the marked region at (a and b) RT, (c and d) 200, (e and f) 400, (g and h) 600, and (i and j) 800 °C

Figures 7.10 (a-c) illustrate the morphology of the worn surfaces of the ball slid against NANGh4 at RT, 400, and 800 ºC. The presence of transfer layer with varying degrees of compaction could be observed on the worn surfaces of ball at different temperatures i.e., RT, 400, and 800 ºC.

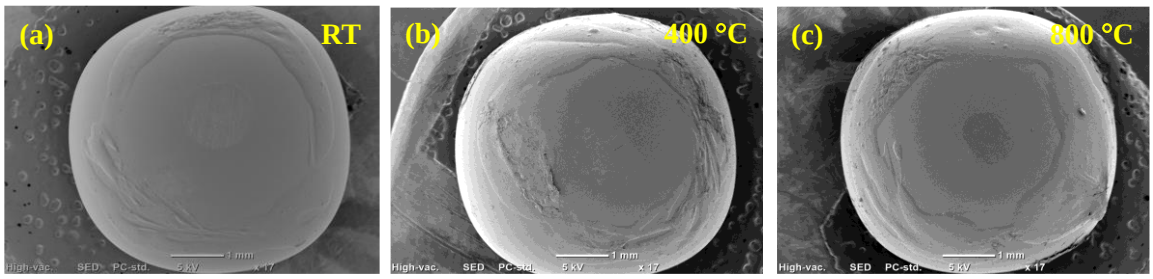

Fig. 7. 10 FESEM micrographs of the worn-out silicon nitride ball (counterface) slid against NANGh4 at (a) RT, (b) 400, and (c) 800 °C

Figures 7.11(a-j) show the FESEM micrographs of the worn surface for NANGh6 at RT, 200, 400, 600, and 800 ºC, along with their EDS. The surface worn at RT shows the presence of a tribo-layer covering almost the entire surface apart from some loose wear particles and ploughing marks as seen from Fig. 7.11 (a), whereas a relatively compact tribo-layer with no signs of ploughing marks could be observed on the surface worn at 200 ºC as depicted in Fig. 7.11 (c). The worn surface at 400 ºC has revealed the presence of a loosely bound tribo-layer covering almost the entire surface apart from some loose wear particles as seen from Fig. 7.11 (e). The worn surfaces of NANGh6 at 600 and 800 ºC show the presence of a glaze layer over the entire surface as seen from Figs. 7.11 (g and i). The EDS analyses of the square regions marked in Figs. 7.11 (a, c, e, g, and i) reveal the presence of constituent elements of the composite and oxygen along with their respective amounts depending on the temperature indicating the possibility of oxidation as evident from Figs. 7.11 (b, d, f, h, and j).

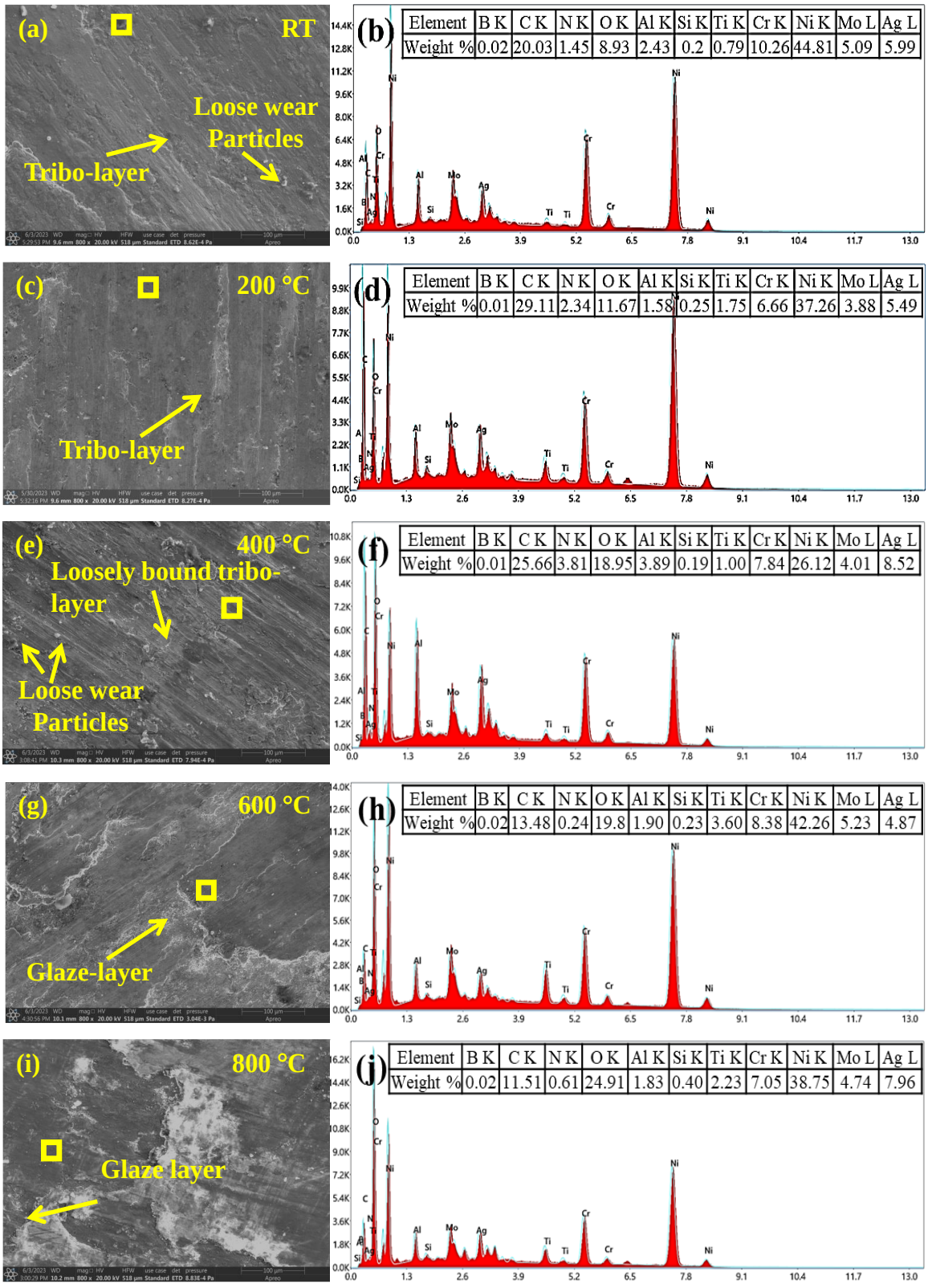

Fig. 7. 11 FESEM micrographs of the worn-out NANGh6 and EDS of the marked region at (a and b) RT, (c and d) 200, (e and f) 400, (g and h) 600, and (i and j) 800 °C

The morphology of the worn surfaces of the ball slid against NANGh6 at RT, 400, and 800 ºC are depicted in Figs. 7.12 (a-c). The wear debris appears to have accumulated at the leading edge of the ball at RT (Fig. 7.12 (a)), whereas a relatively compact and smooth transfer layer can be observed at leading edge of the ball at 400 and 800 ºC (Figs. 7.12 (b and c)).

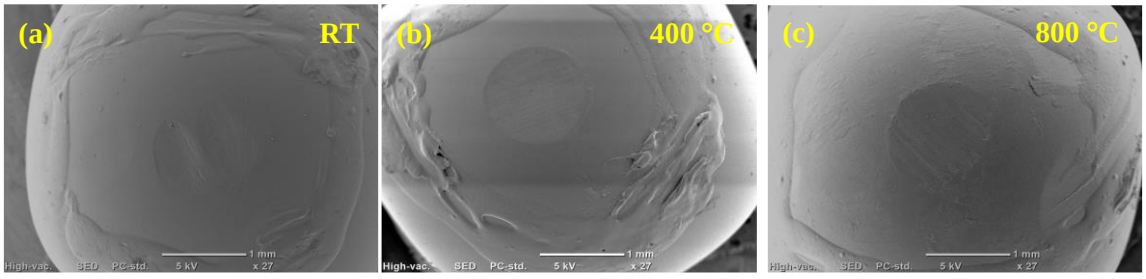

Fig. 7. 12 FESEM micrographs of the worn-out silicon nitride ball (counterface) slid against NANGh6 at (a) RT, (b) 400, and (c) 800 °C

The FESEM micrographs of the surface of NANGh8 worn at RT, 200, 400, 600, and 800 ºC, along with the EDS analyses are shown in Figs. 7.13 (a-j). A compacted tribo-layer covering the sliding marks along with some loose wear particles could be observed on the worn surface of NANGh8 at RT as shown in Fig. 7.13 (a), whereas a tribo-layer covering almost entire worn surface can be seen on at 200 ºC as given in Fig. 7.13 (c). A loosely bound tribo-layer with some signs of delamination can be seen on the surface worn at 400 ºC as shown in Fig. 7.13 (e). On the other hand, the worn surfaces of NANGh8 at 600 and 800 ºC given in Figs. 7.13 (g and i) have revealed the presence of a compacted glaze layer covering the entire worn surface. EDS analyses of the square regions marked in Figs. 7.13 (a, c, e, g, and i) reveal the presence of constituent elements of the composite and oxygen as evident from Figs. 7.13 (b, d, f, h, and j).

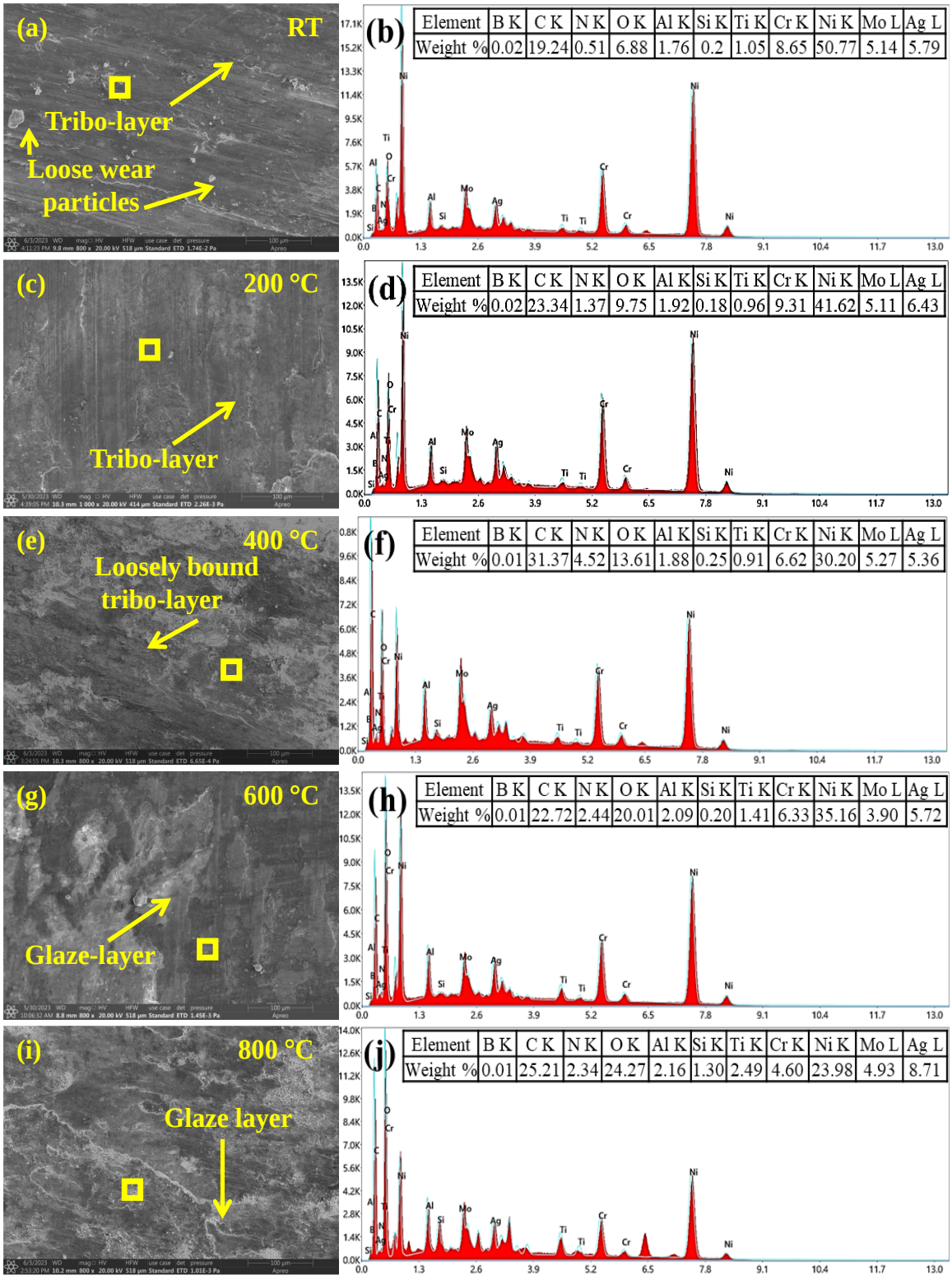

Fig. 7. 13 FESEM micrographs of the worn-out NANGh8 and EDS of the marked region at (a and b) RT, (c and d) 200, (e and f) 400, (g and h) 600, and (i and j) 800 °C

The micrographs of the worn surface of the ball slid against NANGh8 at RT, 400, and 800 °C are illustrated in Figs. 7.14 (a-c). The worn surface at RT shows the wear scar with presence of very little wear debris at the edges as seen from Fig. 7.14 (a) whereas the surface worn at 400 °C shows the presence of relatively more debris at the edge as seen from Fig. 7.14 (b). However, the presence a discontinuous or scattered layer of debris could be seen on the surface of ball worn at 800 °C (Fig. 7.14 (c)).

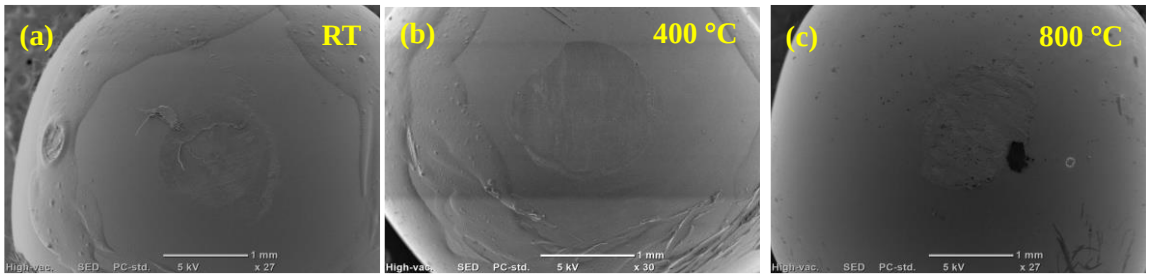

Fig. 7. 14 FESEM micrographs of the worn-out silicon nitride ball (counterface) slid against NANGh8 at (a) RT, (b) 400, and (c) 800 °C

7.1.3.2 X-ray diffraction analysis of the worn surface of composites

Figures 7.15 (a-d) illustrate the XRD patterns of the worn surfaces of NANGh2, NANGh4, NANGh6, and NANGh8, respectively, at RT, 200, 400, 600, and 800 °C. At RT, the worn surface of NANGh2 reveals the presence of the peaks corresponding to *h*-BN, Ag, NiCr, NiAl, and NiTi, whereas an additional peak pertaining to MoO_3 can be seen at 200 °C. The new peaks corresponding to NiO, $NiMoO_4$, and $NiTiO_3$ are observed on the worn surface at 400 °C with no visible peaks belonging to NiCr, NiAl, and NiTi as seen from Fig. 7.15 (a). However, the presence of new peaks pertaining to Ag_2MoO_4 and $Ag_2Mo_2O_7$ could be seen on the surfaces worn at 600 and 800 °C, in addition to the peaks observed at 400 °C. Similar peaks have been observed in the XRD patterns of the worn surfaces of NANGh4, NANGh6, and NANGh8 at all the temperatures as seen for NANGh2 with a

little higher intensity of peaks corresponding to *h*-BN as seen from Figs. 7.15 (b-d).

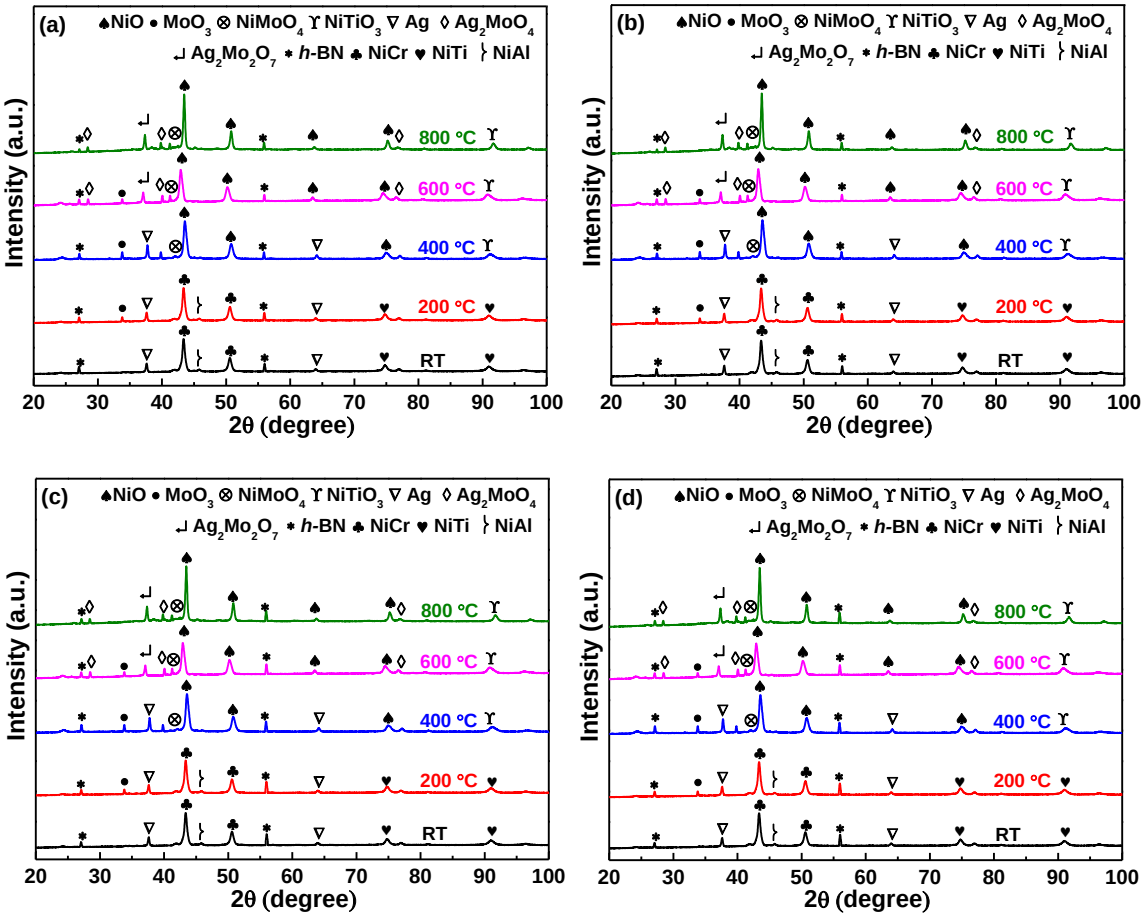

Fig. 7. 15 X-ray diffraction patterns of worn composite (a) NANGh2, (b) NANGh4, (c) NANGh6, and (d) NANGh8 at different temperatures

7.1.3.3 Raman spectroscopy of the worn surface of composites

Raman spectra for the worn surfaces of NANGh2, NANGh4, NANGh6, and NANGh8 at all the temperatures are shown in Figs. 7.16 (a-d), respectively. Raman spectra for the surface of NANGh2 worn at RT and 200 ^{o}C reveal the presence of the peaks corresponding to Al_2O_3, MoC, and *h*-BN. However, new peaks corresponding to MoO_3, Cr_2O_3, NiO, and $NiMoO_4$ at 400 ^{o}C and $Ag_2Mo_2O_7$ at 600 and 800 ^{o}C could be observed on the worn surface in addition to those seen at 200 ^{o}C as evident from Fig. 7.16 (a). A similar pattern of peaks with a relatively higher intensity for the peak pertaining *h*-BN is observed

for NANGh4, NANGh6, and NANGh8 as seen from Figs. 7.16 (b-d).

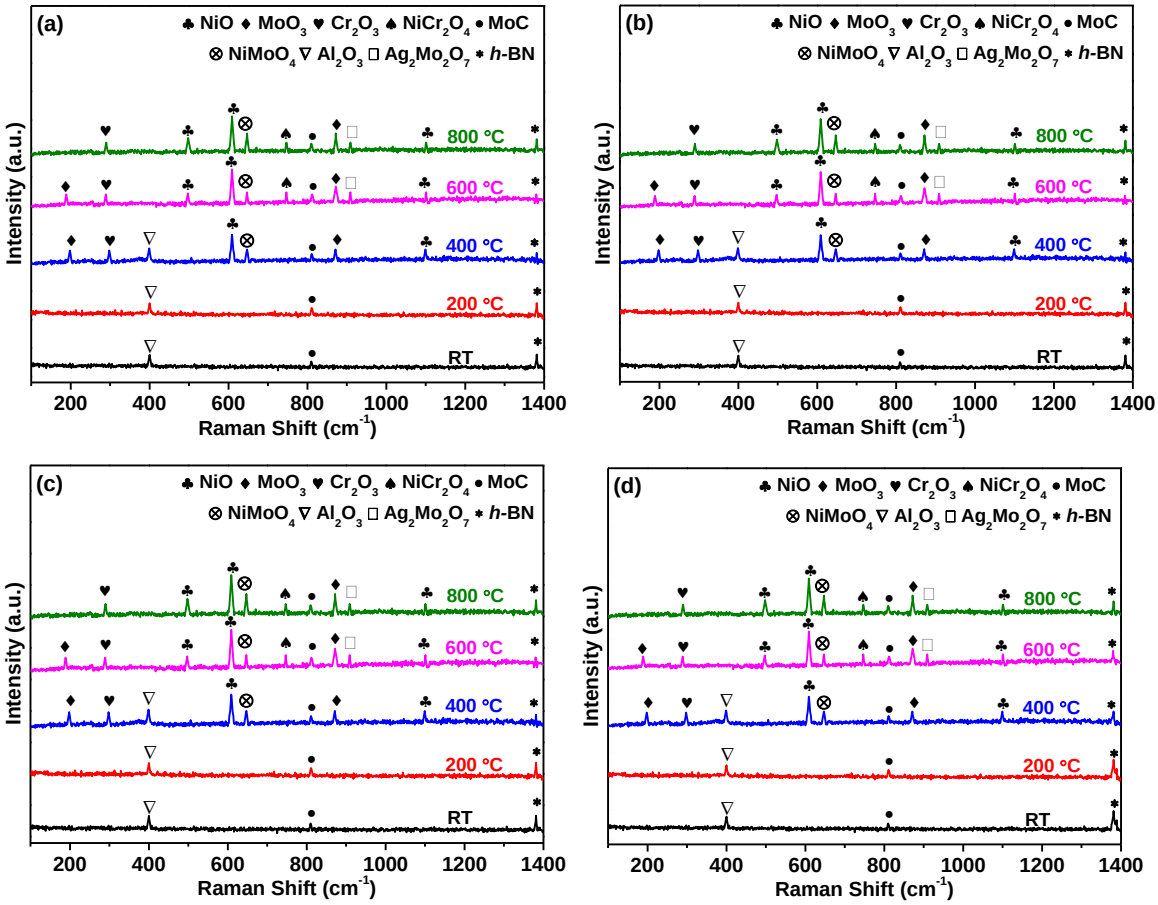

Fig. 7. 16 Raman spectra of worn surface of (a) NANGh2, (b) NANGh4, (c) NANGh6, and (d) NANGh8 at different temperatures

7.1.3.4 Examination of Subsurface

FESEM images of the cross-section of the surfaces of nanocomposites worn at 800°C as shown in Figs. 7.17 (a-d) confirm the presence of a glaze-layer. The average thickness of glaze-layer for NANGh2, NANGh4, NANGh6, and NANGh8 is 179.0, 188.3, 186.6, and 191.5 µm, respectively. The thickness of the glaze-layer has also been observed to increase with increasing amount of *h*-BN from 2 to 8 wt.%.

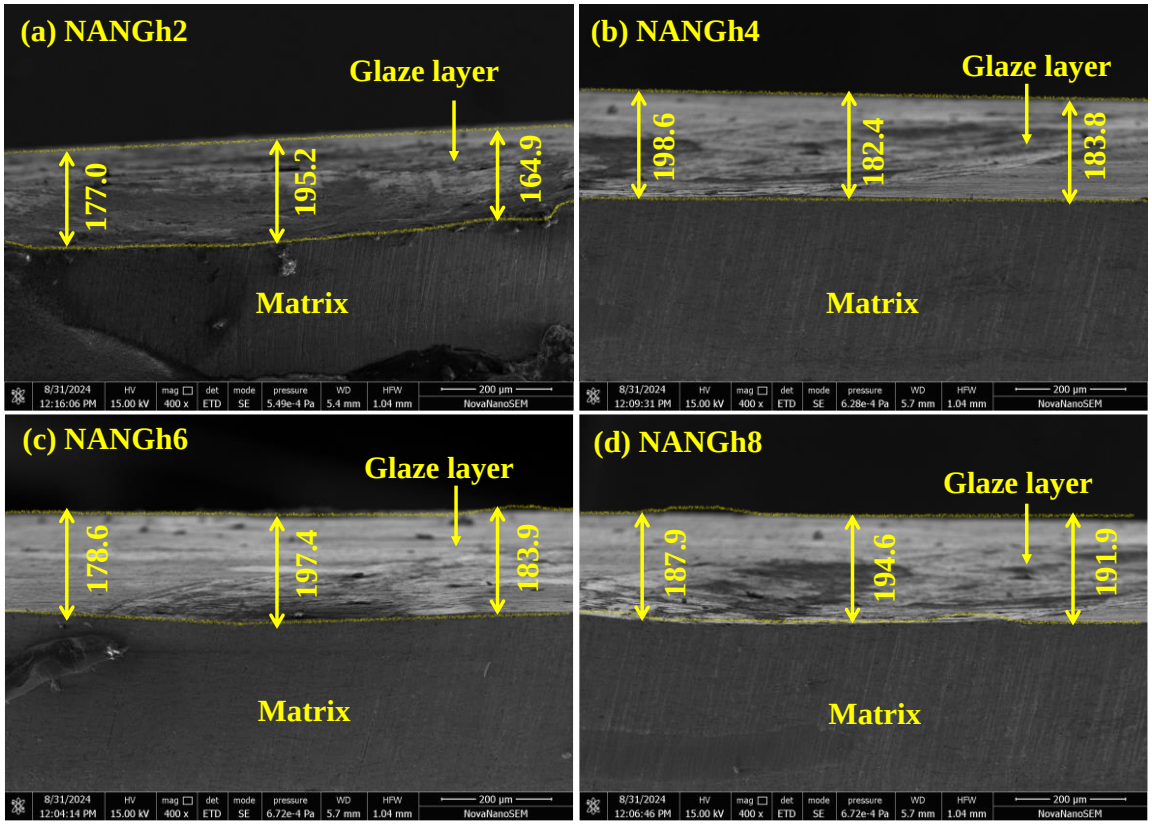

Fig. 7. 17 FESEM micrographs of cross-section of subsurface of worn track at 800 °C corresponding to (a) NANGh2, (b) NANGh4, (c) NANGh6, and (d) NANGh8

7.2 DISCUSSION

The increase in the amount of Ni-doped *h*-BN from 2 to 8 wt.% in the composites results in decrease in the hardness of the composites from 458 ± 3 to 412 ± 2 $HV_{0.3}$, mainly due to the inherent softness of *h*-BN [100]. A decrease in hardness with increasing amount of *h*-BN has also been reported by Feng et al.[114] in Ni-Cr matrix based composites whereas, Elkady et. al [117] and Gnanavelbabu et al.[118] have reported the same in the case of Cu-based composites.

The higher stability in CoF over time for the composites containing a combination of Ag, rGO, and *h*-BN at all the temperatures compared to base alloy (N0), the composite

having Ag, the combinations of Ag/rGO, i.e., NANG, might be due to formation of tribo-layer on the worn surface leading to uniform pressure distribution at the interface of mating pairs during sliding.

In Chapters 4, 5, and 6, the effect of the addition of a single or a combination of solid lubricants, namely, Ag, Ni-doped rGO and Ni-doped *h*-BN in Ni alloy-based composites (N0) has been discussed for attaining effective lubrication from RT to 800 ºC. The CoF of the base alloy, i.e., N0 has been found to decrease from (~ 0.71- 0.38) to (~ 0.67- 0.36) with the addition of 10 wt.% Ag, i.e., for NA from RT to 800 ºC. A further addition of 1 wt.% Ni- doped rGO in NA i.e., NANG results in a reduction in COF from (~ 0.67 – 0.50) to (~ 0.59 - 0.46) from RT to 600 ºC. However, at 800 ºC, the CoF of NANG has been found to be relatively high (~ 0.45) than both N0 (~ 0.38) and NA (~ 0.36). The decrease in the CoF for NANG from RT to 600 ºC has been attributed to the assistive action between a combination of solid lubricants i.e., Ag and Ni-doped rGO, whereas a higher CoF at 800 ºC has been ascribed to the loss of lubricity of rGO and simultaneous suppression of efficacy of the lubricious oxides and molybdates as discussed in chapter 4. The addition of 8 wt.% Ni-doped *h*-BN in NA resulted in a reduction in CoF from (~ 0.67-0.36) to (~ 0.48 - 0.18) from RT to 800 ºC which has been credited to the synergistic action between Ag and *h*-BN as explained in chapter 6.

In the present Chapter, the potential of a combination of all the three lubricants i.e., Ag, Ni-doped rGO, and Ni-doped *h*-BN has been explored to achieve low friction and low wear properties from RT to 800 ºC. The CoFs of all the composites containing different amounts of *h*-BN i.e., NANGh2, NANGh4, NANGh6, and NANGh8 have been found to

decrease continuously from RT to 800 ºC as seen from Fig. 7.5. The CoF values for NANGh2, NANGh4, NANGh6 have been found to lie in a narrow band whereas NANGh8 has shown a significantly lower CoF than these composites at all the temperatures. The decrease in CoF with increasing temperature may be credited to the presence of tribo-layer containing lubricating components i.e., Ag, *h*-BN, and NiO, at RT and 200 ºC; additionally, MoO_3 and $NiMoO_4$ at 400 ºC and Ag_2MoO_4, and $Ag_2Mo_2O_7$ at 600 and 800 ºC as evidenced by the XRD (Figs. 7.15 (a-d)) and the Raman spectra (Figs. 7.16 (a-d)) which endows the interface with easy shearing capability and helps in restricting the junction growth despite their low hardness. At a particular temperature, the CoF has been observed to decrease with increasing amount of *h*-BN as seen from Fig. 7.5 and NANGh8 has shown the lowest CoF (~ 0.26 - 0.17) at all the temperatures, which may be attributed to a relatively higher amount of *h*-BN in this composite. To further analyse the reasons for a significantly lower CoF shown by NANGh8 than NANGh2, NANGh4, and NANGh6 the cross-section of the specimen worn at 800 ºC has been analysed for determining the thickness of the tribo-layer. The results indicate a relatively larger thickness of tribo-layer for NANGh8 in comparison to others as seen from Figs. 7.17 (a-d), which might also have helped in reducing the friction.

Among all the materials mentioned above, the one containing a combination of all the three lubricants i.e., Ag, Ni-doped rGO and Ni-doped *h*-BN has consistently shown a lower CoF at all the temperatures which reflects the occurrence of a synergistic action between Ag, rGO, and *h*-BN wherein Ag, being a low-temperature lubricant is assisted by rGO, a room to moderate temperature lubricant and *h*-BN, which is considered an excellent high temperature lubricant with high thermal stability as reported by others also

[39,42,100].

The variation of wear rate for N0, NA, and NANG with temperature as seen in Fig. 7.6 has been explained in Chapter 4 on the basis of the relative dominance of the hardness, effectiveness of the transfer layer containing lubricious species, and extent of cover provided by the transfer layer to the underlying substrate. However, the comparatively lower wear rates of NA and NANG in comparison to N0 at all temperatures have been attributed to the lubricating action of Ag and its molybdates in NA and assistive action between Ag and rGO in NANG.

The variation of wear rate of NANGh2, NANGh4, NANGh6, and NANGh8 from RT to 800 ºC (Fig. 7.6) may be explained on the basis of the softening of the material with increasing temperature and features such as the presence loose wear particles, nature of tribo-layer (compact/loosely bound and continuous/scattered) and regions of delamination visible on the worn surfaces of the composites as discussed in Chapters 4, 5, and 6. An increase in wear rate from RT to 400 ºC for these composites may be elucidated based on the comparison of FESEM images of surfaces worn at these temperatures which present a relatively continuous and compact tribo-layer at RT and a loosely bound and scattered layer with varying degrees of compaction apart from some locations of delamination at 200 and 400 ºC as seen from a comparison of Figs. 7.7, 7.9, 7.11, and 7.14 (a, c, and e). The presence of a scattered tribo-layer and regions of delamination allow direct contact between the tribo-pair, leading to an increase in material loss. A decrease in wear rate at 600 ºC may be attributed to the formation of a glaze layer as evident from Figs. 7.7, 7.9, 7.11, and 7.13 (g). The formation of glaze has been shown to be effective in reducing both friction and wear

at elevated temperatures [119–121]. The decrease in wear rate at 800 ºC despite a reduction in the hardness due to softening indicates the dominating effect of the glazed layer over the decreasing hardness. The wear rate for NANGh2, NANGh4, NANGh6, and NANGh8 have been observed to lie in a narrow band with NANGh6 showing the lowest wear rate than others at all the temperatures.

A consistently lower wear rate shown by the composites NANGh2, NANGh4, NANGh6, and NANGh8 in comparison to N0 and NA at all the temperatures may be attributed to the presence of a well-established glaze layer present on their worn surfaces apart from the synergistic action of Ag, rGO, and *h*-BN reflecting the effectiveness of these over the reduced hardness. However, the wear rate for these composites and NANG are found to lie in a narrow band (~ 4.4 - 8.4 × 10^{-5} mm^3/Nm) with slight variations based on composition and working temperature controlled by the interplay between synergistic action of lubricants and hardness of composites.

Based on the characteristics of the surfaces worn under different temperatures it may be inferred that the abrasion and ploughing are the dominant wear mechanisms at RT and 200 ºC, whereas wear appears to have occurred by a combination delamination, ploughing and oxidation at 400 ºC. However, at 600 and 800 ºC oxidation seems to be the dominant mechanism as revealed by the presence of glaze. The schematic illustration depicting the wear mechanism of the nanocomposites as given in Fig. 7.18, demonstrates the occurrence of possible tribo-chemical reactions during sliding at the interacting surfaces based on the observed friction and wear behaviour the morphology of the worn surfaces of the tribo-pairs under FESEM along with their XRD and Raman spectra. The presence of

tribo-layer rich in Ag and *h*-BN and covering almost the entire worn surface of the composite, is responsible for the reduction of friction from RT to 200 ºC. The existence of a scattered tribo-layer having lubricious oxides such as NiO, MoO_3, and $NiMoO_4$, along with Ag and *h*-BN on the worn surface of the composites at 400 ºC, might have further reduced friction, whereas the direct contact between the composite and counter ball must have increased the loss of material. However, at 600 and 800 ºC, the formation of a smooth and compact glaze layer enriched with Ag, *h*-BN, NiO, MoO_3, $NiMoO_4$, Ag_2MoO_4, and $Ag_2Mo_2O_7$ over the worn surfaces of the tribo-pairs must have played an instrumental role effectively reducing both CoF and wear rate for the nanocomposite. These observations suggest a cooperative synergy between Ag, rGO, and *h*-BN in effectively reducing friction and wear at temperatures beyond 400 ºC.

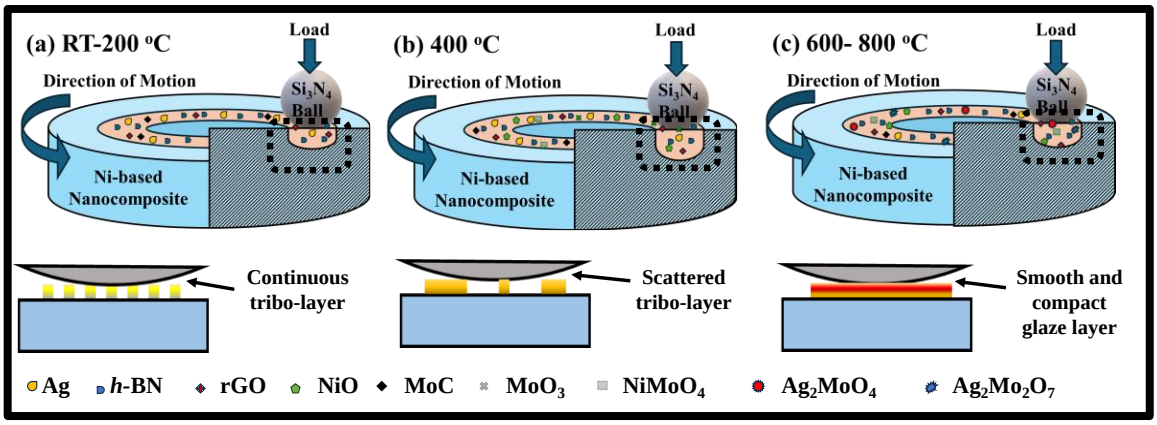

Fig. 7. 18 Schematic illustration for the wear mechanism of Ni alloy-based nanocomposites at (a) RT, (b) 400, and (c) 800 ºC

To summarise, a novel combination of solid lubricants e.g., Ag, Ni-doped rGO, and Ni-doped *h*-BN in Ni-alloy based composites is able to achieve low friction (~ 0.39 - 0.17) and low wear properties (~ 4.4 - 8.4 $\times 10^{-5}$ mm^3/Nm) under extended regime of temperatures

from RT to 800 ^{o}C. However, the composite NANGh8 containing 10 wt.% Ag, 1 wt.% rGO-Ni, and 8 wt.% *h*-BN, showed the lowest coefficient of friction (~ 0.27- 0.17) at all the temperatures due to relatively larger amount of *h*-BN and the synergistic action of Ag, rGO, and *h*-BN.